SAR Generated by Commercial Cellular Phones—Phone Modeling, Head Modeling, and Measurements

Andrea Schiavoni, *Member, IEEE*, Paola Bertotto, Gabriella Richiardi, and Paolo Bielli

***Abstract*—This paper presents the computation of the specific absorption rate (SAR) generated by cellular phones inside an anatomical model of a head. Four models of commercially available phones have been considered working at 900- and 1800-MHz bands (global system for mobile communication system). The phones have been modeled by using a computer-aided design representation obtained through the reverse engineering technique. Both SAR distributions and SAR averaged values have been computed inside the anatomical model of a head, by using the finite-difference time-domain method. Computations have been experimentally validated through measurements performed inside anthropomorphic phantoms irradiated by a dipole and cellular phones.**

***Index Terms*—Anthropomorphic phantom, CAD modeling, cellular phone, anatomical head, FDTD, SAR measurements.**

I. Introduction

THE advantages of analyzing specific absorption rate (SAR) generated by cellular phones inside a human head are, among others, as follows:

- verification of the compliance of phones with standards [1], [2];
- electromagnetic solver, experimentally validated, gives not only reliable values of specific absorption rate (SAR), but also locations inside a head [3]–[10];
- high resolution in field evaluation could be of interest, as input data, for the analysis of athermal effects [11].

The most used method to solve the electromagnetic problem dealt with this area is the finite-difference time-domain (FDTD) technique [12], [13]. Although, in principle, the solution for general geometries does not require any additional effort with respect to the standard method, the technique requires the definition of the discretized space by assigning to each cell its own electromagnetic properties, which is not an easy process [9], [10], [14], [15]. Specifically, the problems to be solved in SAR evaluations are as follows:

- correct representation of the cellular phone;
- anatomical representation of the head;
- alignment of the phone and the head.

The use of computer-aided design (CAD) representation of a phone [14] is very effective both to avoid errors in modeling and to allow fast processing, but CAD models are not always available. In order to overcome this obstacle, the reverse engineering (RE) technique has been used to get the CAD representation of any cellular phone and, in general, of any kind of object.

The numerical model of a human head is based on magnetic resonance (MR) images. As long as MR images cannot be directly used by the electromagnetic solver, they have to be transformed in an anatomical image, replacing voxels with labels representing tissues [16].

The numerical model of the phone and head have to be aligned with each other, in the discretized space, in a defined position [1], this process cannot be performed manually, and a mesher had be used instead.

The validation of the electromagnetic solver is an important task to be done so that the field computed inside a head is reliable. A great effort has been done by the scientific community in the past[1] and the validation is effective if performed in a realistic situation.

Four cellular phones, all equipped with whip antennas, have been analyzed. Even though whip antennas do not represent an exhaustive set of commercially available antennas (helix, planar antennas), it is beyond the scope of this paper to analyze all possible antenna solutions.

II. Modeling

SAR computation by means of the FDTD technique requires the description of both the phone and human head in a discretized space. A mesher able to solve this problem has been developed. The geometry of the phone and the model of a head are input to the mesher, which performs the alignment and discretizes the space.

A. Phone Modeling

To get an accurate model of a phone in a discretized space, the representation of all the details of interest must be available, such as the keyboard, the display, and the phone's case. One of the main problems related to the description of cellular phones is the acquisition of the external geometry. The presented approach is based on the RE technique [17]; by using this approach, it is not necessary to have any mechanical CAD drawing of the phone; the procedure itself will create it, allowing each kind of object to be modeled. Cellular phones are very

Manuscript received November 10, 1999; revised May 3, 2000. This work was supported by Telecom Italia Mobile.

The authors are with the Centro Studi e Laboratori Telecomunicazioni, 10148 Turin, Italy.

Publisher Item Identifier S 0018-9480(00)09698-8.

[1][Online]. Available http: www.radio.fer.hr/cost244

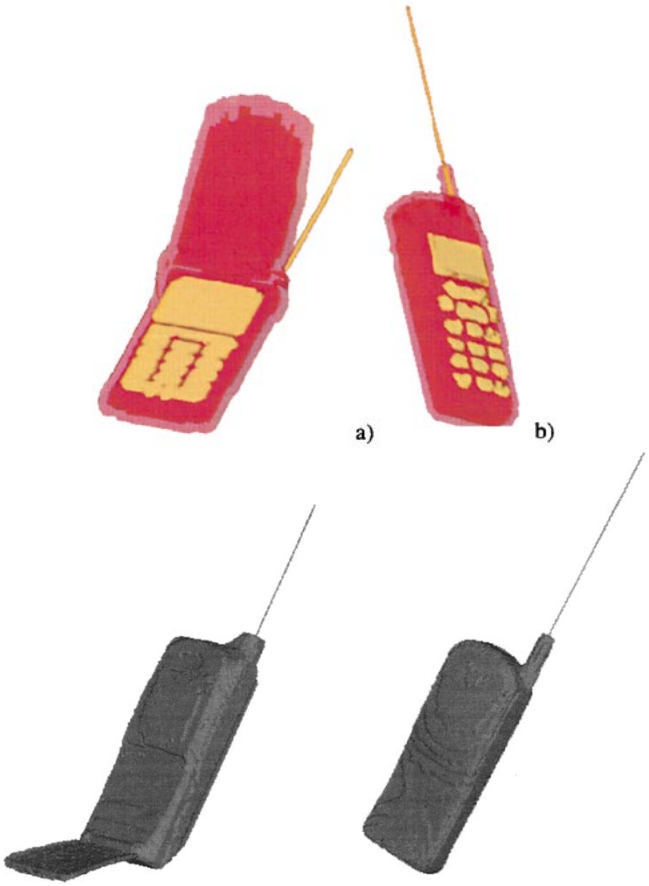

Fig. 1. (a)–(b) Discretized models of GSM phones. (c) 900- and 1800-MHz dual band.

often modeled as metallic boxes, resulting in a representation not effective for commercial phones. A description of the differences in electromagnetic behavior between an accurate model of a phone and its approximated model can be found in [17].

The RE technique consists of the following two steps.

Step 1—3-D Scanning: A three-dimensional (3-D) topometric sensor, based on two cameras, acquires the geometry. The 3-D coordinates are computed for each point by using triangulation methods and image processing; the object, at this step, is represented as a cloud of points.

Step 2—Mathematization: The cloud of points is used to create the surface describing the external skin of the object. The surface is transformed into a grid of triangular patches and stored in a CAD file; different parts are distinguished by colors.

The RE process represents only the external case of the phone; no internal structure is described; the phone is then represented as a plastic shell filled by metal, as shown in Fig. 1. The possible influence on the SAR of the internal circuitry is open to question. Anyway, the impact of the phone's internal modeling on the computation, which has to be traded off with the increased field precision, can be summarized as follows:

- CAD representation of the phone's internal structure;
- modeling of the internal parts, with a probable decrease of the space discretization step dimension;
- localization and characterization of the sources inside the case.

TABLE I
RECOGNIZED TISSUES IN THE HEAD MODEL

White Matter	Eye	Optic Nerve	Crystalline Lens
Grey Matter	Muscle	Teeth	Choroid Plexus
CSF	Skin	Rhino-pharynx	Marrow
Blood	Compact Bone	Cartilage	Acoustic Nerve
Fat	Cancellous Bone	Falx cerebri	Hypophysis
Parotid Gland	Mucous	Tongue	Truncus Cerebri
Caudate Nucleus	Corpus Callosum	Thalamus	Mammillary Bodies
Lenticular Nucleus	Pileum	Chiasma	Vermis Cerebelli
Pineal Gland	Anterior Commissure	Lachrymal Gland	Internal Air

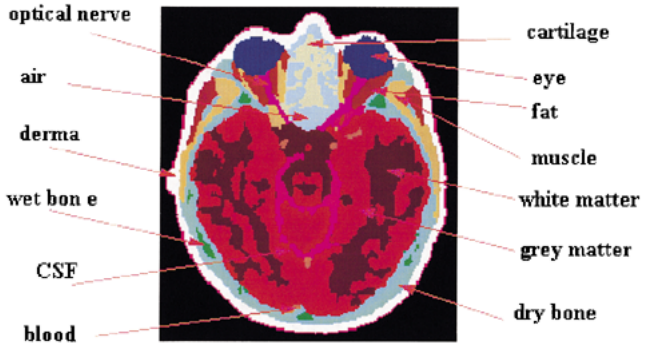

Fig. 2. Labeled slice at eye level.

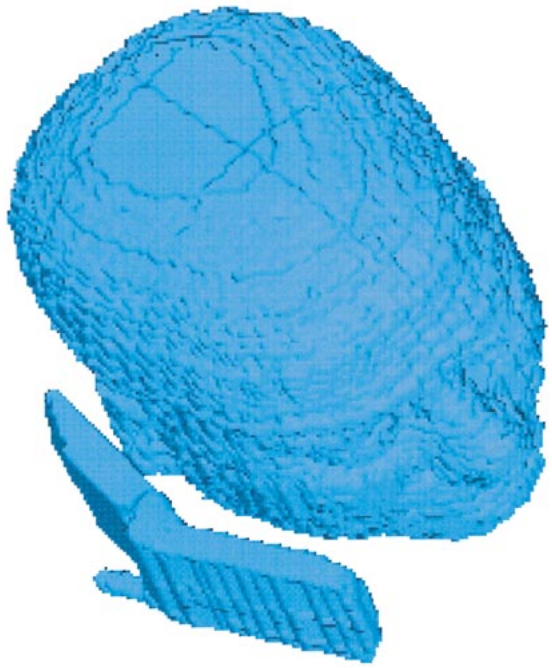

Fig. 3. GSM cellular phone [see Fig. 1(a)] aligned in the "Intended Use" position to the 3-D model of a head in the discretized space.

B. Head Modeling

The anatomical model of the head has been obtained by acquiring an MR image. The set of original images consists of 90 slices; the dimension of the voxel is $0.97 \times 0.97 \times 2$ mm^3. The MR image has been: 1) elaborated numerically, by means of a neural-network approach, to associate each voxel with a label

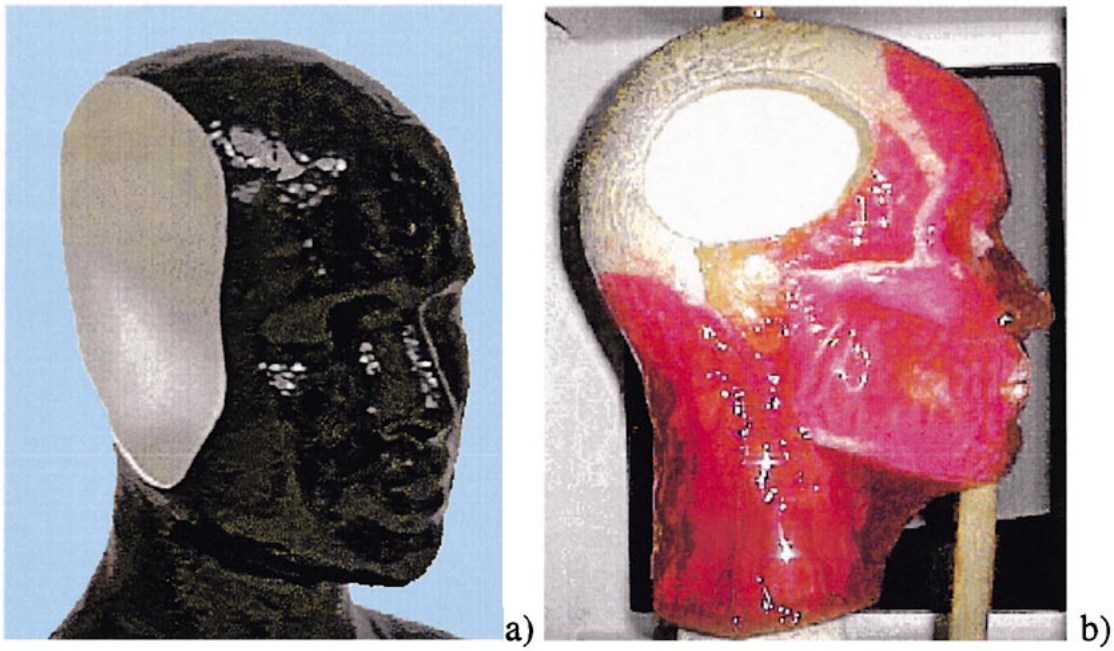

Fig. 4. (a) Homogeneous phantom. (b) Inhomogeneous phantom. The numerical models of phantom have been obtained by means of an MR acquisition of the mannequin.

representing a tissue [16] and 2) validated by radiologists and neurologists.

In the head model, 36 tissues have been distinguished (see Table I) and Fig. 2 shows a slice at the eye level. Starting from the labeled image, the association of the physical constants is straightforward to obtain the electromagnetic model of the head [10], [18], [19].

C. Mesher

The mesher, developed at the Centro Studi e Laboratori Telecomunicazioni (CSELT), Turin, Italy, is able to manage data in the format described in the previous points [17]. Inputs to the mesher are the FDTD space discretization step and the geometrical coordinates necessary to align the phone with the head. It automatically performs the alignment and generates the discretized space. Fig. 3 shows a phone aligned to the head in the discretized space.

D. Electromagnetic Problem

The use of the FDTD technique has solved the electromagnetic problem; the electromagnetic description of the space is done by the mesher through the assignment of the electromagnetic constants to each cell. To represent the discretized space in the computer's memory, surfaces are truncated so as to limit the FDTD grid by using the retarded time absorbing boundary condition (ABC) [20]. As long as the standard FDTD does not allow discriminating objects having dimensions smaller than the space discretization step, an analytical approach has been used to describe the field around thin wires [13] in the simulation of whip antennas. The power has been evaluated by using the Poynting's theorem.

III. SAR Measurements

The measurement setup [21], [22] consists of a six-axis robot moving an electric-field probe inside a phantom representing a head; the phantom is filled with a liquid simulating the electromagnetic properties of the brain.

The brain equivalent liquid has been obtained by following the recipe proposed in [23]. The permittivity and conductivity of the liquid have been measured with an HP 85070B system [24] and they are used as input data both for measurements and computations.

An SAR measurement consists of the following three steps.

Step 1) *Coarse grid scan*. The area corresponding to aperture on the side of the phantom is scanned. The goal is the localization of the SAR peak value.

Step 2) *Cube measurement*. Once the position of the peak has been found, the SAR is measured in a cubic volume big enough to evaluate the SAR values averaged on 1 and 10 g.

Step 3) *Penetration curve*. Once the probe position has been defined on the phantom's surface, the field is measured moving back the probe on a straight line.

The uncertainty associated with the SAR measurement [25] is about $\pm 25\%$ with a confidence level of 95%, depending on the values of conductivity and density. Since the side dimension of the cube, on which SAR is averaged, depends on the density, it is important to its value.

IV. Validation

The validation process consists of a comparison between the measured and computed SAR inside two anthropomorphic phantoms radiated either by a calibrated dipole or by commercially available phones. The European Standard [1] indicates

TABLE II
ELECTROMAGNETIC CHARACTERISTICS OF THE MATERIALS CONSTITUTING THE PHANTOMS

Material	Permittivity	Conductivity [S/m]
Inhomogeneous Phantom		
Skin	42.0	0.80
Bone	14.7	0.14
Muscle	51.7	1.13
Eye	69.4	1.62
Liquid Brain	Measured	Measured
Homogeneous phantom		
Fiberglass	2.4	0.0
Liquid Brain	Measured	Measured

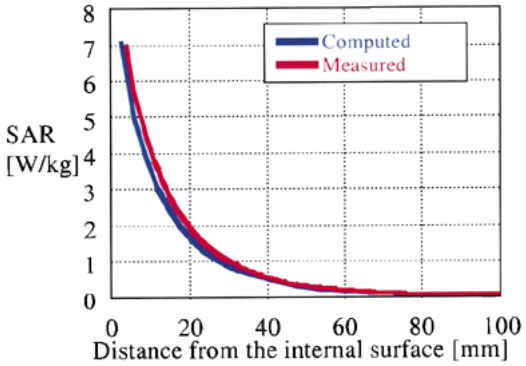

Fig. 5. Homogeneous phantom and dipole: penetration curve.

four phantoms: the "homogeneous" phantom [1, homogeneous torso] and the "inhomogeneous" phantom [1, inhomogeneous phantom] have been considered (see Fig. 4) and the cranial cavity has been filled with the brain equivalent liquid [23].

Both phantoms have been modeled as described previously for the head. The electromagnetic characteristics of each matter constituting phantoms are listed in Table II.

A. Phantoms Irradiated by a Dipole

The ANRITSU Model MP651B calibrated dipole has been used as the source; at 900 MHz, the length of the dipole is 156 mm with a medium arms' radius of 3 mm. The two arms are connected to a plastic box; the distance between the center of the arms and the surface of the box is 8 mm. The dipole has been connected to an RF signal generator, an amplifier, and a bi-directional coupler to measure both the direct and reflected powers.

The first test consists of the homogeneous phantom irradiated by the dipole placed vertically. A radiated power of 600 mW in free space has been considered (the power radiated by a TACS phone); the radiated power when the dipole is in contact with the central point of the ear on the phantom is 522 mW. The characteristics of the brain equivalent liquid were $\varepsilon_r = 40.36$ and $\sigma = 0.89$ S/m $p = 1.28$ g/cm^3; the space has been discretized into 3-mm cubic cells. Fig. 5 shows the comparison between the measured and computed SAR on the penetration curve. The relative difference, reported in Table III, has been evaluated as

$$\Delta = \frac{\mathrm{SAR}_{\mathrm{computed}} - \mathrm{SAR}_{\mathrm{measured}}}{\mathrm{SAR}_{\mathrm{measured}}} 100. \qquad (1)$$

The second example consists of the dipole placed vertically close to the inhomogeneous phantom. The position of the dipole has been chosen in order to place the maximum of the SAR in correspondence of the center of the side aperture of the phantom. The attenuation of the electromagnetic field is higher than in the previous test; to prevent too low signals inside the liquid, a radiated power in free space of 1 W has been considered. When the dipole is into contact with the phantom, the radiated power is 1.24 W. The space discretization step is 3.4 mm, while the brain equivalent liquid has the following characteristics: $\varepsilon_r = 40.3$, $\sigma = 0.86$ S/m 1.28 g/cm^3. Fig. 6 shows the comparison on the penetration curve and Table III reports the SAR values.

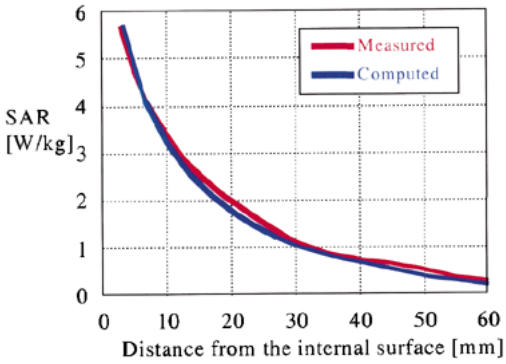

Fig. 6. Inhomogeneous phantom and dipole: penetration curve.

TABLE III
SAR COMPARISON INSIDE THE PHANTOMS RADIATED BY THE DIPOLE

	SAR_{max} [W/kg]	Δ [%]	$SAR_{1.0g}$ [W/kg]	Δ [%]	$SAR_{10.0g}$ [W/kg]	Δ [%]
Homogeneous phantom						
Measured	6.98	1.3	6.52	0.8	4.04	-5.4
Computed*	7.07		6.57#		3.82	
Inhomogeneous phantom						
Measured	5.70	0.2	4.81	16.0	3.10	8.1
Computed*	5.71		4.04		2.85	

SAR_{max} measured corresponds to SAR with the probe as close as possible to the internal surface of the phantom. Between the detecting dipoles and the surface there is a distance of about 4 mm large [22-23] where SAR increases exponentially; the measurement system extrapolates SAR values on this gap for SAR averaging. SAR_{max} computed is evaluated at this position.
* The averaging volume is defined in a discretized space. These values have been obtained linearly interpolating SAR averaged over the nearest cubes having a mass less than and greater than the 1.0 or 10.0 g.

B. Phantoms and Commercial Phones

Two commercially available global system for mobile communication (GSM) phones have been considered. The phones are set to radiate at the maximum power at 900 MHz. The measured peak power irradiated at that frequency was 30 dBm (±0.5 dB) for phone A, equipped with a $\lambda/4$ antenna [see Fig. 1(a)], and 30.5 dBm (±0.5 dB) for phone B, equipped with a $3/8\lambda$ antenna [see Fig. 1(b)]. Both phones have been aligned to the phantom according to the "intended use" position [1]. The space has been discretized into 2.0-mm cubic cells; the electromagnetic characteristics of the liquid were $\sigma = 0.84$ S/m and $\varepsilon_r = 39.8$ $p = 1.28$ g/cm^3 for the homogeneous phantom and $\sigma = 0.86$ S/m and $\varepsilon_r = 40.3$ $p = 1.28$ g/cm^3 for the inhomogeneous phantom, respectively. Table IV shows a comparison between the measured and computed SAR, while Fig. 7 shows a comparison between SAR distribution inside the homogeneous phantom for phone B.

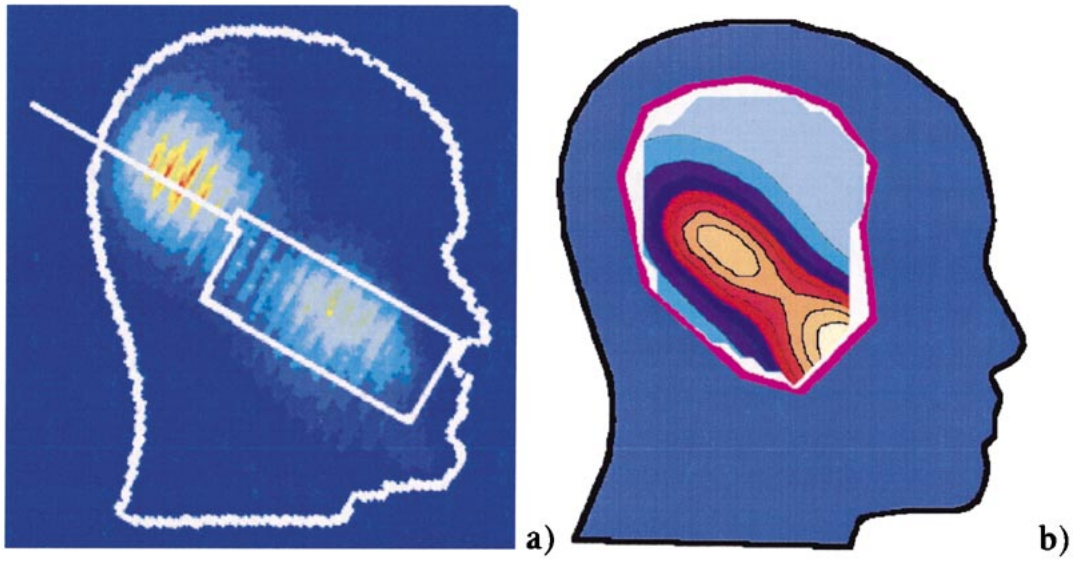

Fig. 7. Homogeneous phantom and phone B. (a) Computed SAR distribution. (b) Measured SAR distribution.

TABLE IV
MEASURED AND COMPUTED SAR VALUES FOR PHONES A AND B

			Homogeneous Phantom	Δ [%]	Inhomogeneous Phantom	Δ [%]
Phone A						
$SAR_{1.0g}$	[W/kg]	Measured	0.12	0	0.02*	-
		Computed	0.12		0.05	
$SAR_{10.g}$	[W/kg]	Measured	0.07	12.5	0.01*	-
		Computed	0.08		0.03	
Phone B						
$SAR_{1.0g}$	[W/kg]	Measured	0.12	8.3	0.09	-22.2
		Computed	0.13		0.07	
$SAR_{10.g}$	[W/kg]	Measured	0.08	12.5	0.06	-16.7
		Computed	0.09		0.05	

*values below the sensibility of the probe

SAR distributions inside the phantoms are different due to the following:

- shape and dimensions of the phantoms; the homogeneous is bigger than the inhomogeneous;
- homogeneous phantom does not have the ear, thus, the source is closer to the internal liquid;
- side aperture of the inhomogeneous phantom is smaller than the aperture of the homogeneous and it is limited to the cranial cavity;
- inhomogeneous phantom has an absorbing ear, and between the liquid brain and external surface there are two absorbing layers; the shell of the homogeneous phantom practically does not introduce any attenuation, except for thickness.

This results in a lower SAR value inside the inhomogeneous phantom. It can be observed that even if there is a satisfactory agreement on $\mathrm{SAR}_{1.0\mathrm{g}}$, since measured values are greater than the sensitivity of the probe, the agreement is worse on $\mathrm{SAR}_{10.0\mathrm{g}}$ since more low SAR points, below probe sensitivity, are considered.

V. SAR INSIDE A HUMAN HEAD

Four commercially available GSM phones have been considered (Fig. 1), and the SAR has been computed by assuming that each phone radiates a peak power of 33 dBm at 900 MHz or 30 dBm at 1785 MHz. The phones are distinguished according to their antenna length: Phone A—92 mm, Phone B—126 mm, Phone C—85 mm, and Phone D 143 mm.

The space has been discretized into 2.0-mm cubic cells for phones A and B, and 1 mm for phones C and D. Each phone has been modeled as a plastic shell ($\varepsilon_r = 2.4$, $\sigma = 0.0$ S/m) filled with metal; on the shell, the keyboard and display are evidenced. The values for the conductivity and permittivity reported in [10], [18], and [19] have been used for the electromagnetic model of the head. Table V shows the computed SAR. The column $\mathrm{SAR}_{\mathrm{peak}}$ gives the maximum SAR found in a cell of the discretized space. The column $\mathrm{P}_{\mathrm{abs}}$ is the ratio between the total radiated power and the power absorbed by the head. Table VI shows SAR percentage of each tissue of the head (above 1%) computed as

$$\mathrm{SAR}_{\%} = \frac{\sum \mathrm{SAR}(z,y,x)|_{\mathrm{tissue}}}{\sum \mathrm{SAR}(z,y,x)|_{\mathrm{head}}} 100. \tag{2}$$

SAR percentages do not take into account how the SAR distributes inside the head, but indicate what tissue is mostly affected by the radiation. Total absorbed power and power density are not exactly taken into account for SAR distribution.

The skin is shown to be the tissue mostly involved by radiation, with an increase at 1785 MHz due to the reduction of the penetration depth. Also, the antenna's length play a role in SAR distribution; phone A and C at 900 MHz have a lower impact on both gray and white matter. Phones B and D have a longer antenna, moving the radiation toward the back of the head; in this case, the shield effect of the external layers is lower due to the lower thickness. This does not mean that the SAR is higher. Quarter-wavelength antennas concentrate the radiation mostly in the ear region; hence, involving the muscle, skin, and parotid above all. Fig. 8 shows the SAR distribution normalized to the maximum SAR; the concepts explained above can be observed in this figure. The SAR has been reported in log scale since it decays exponentially inside the head.

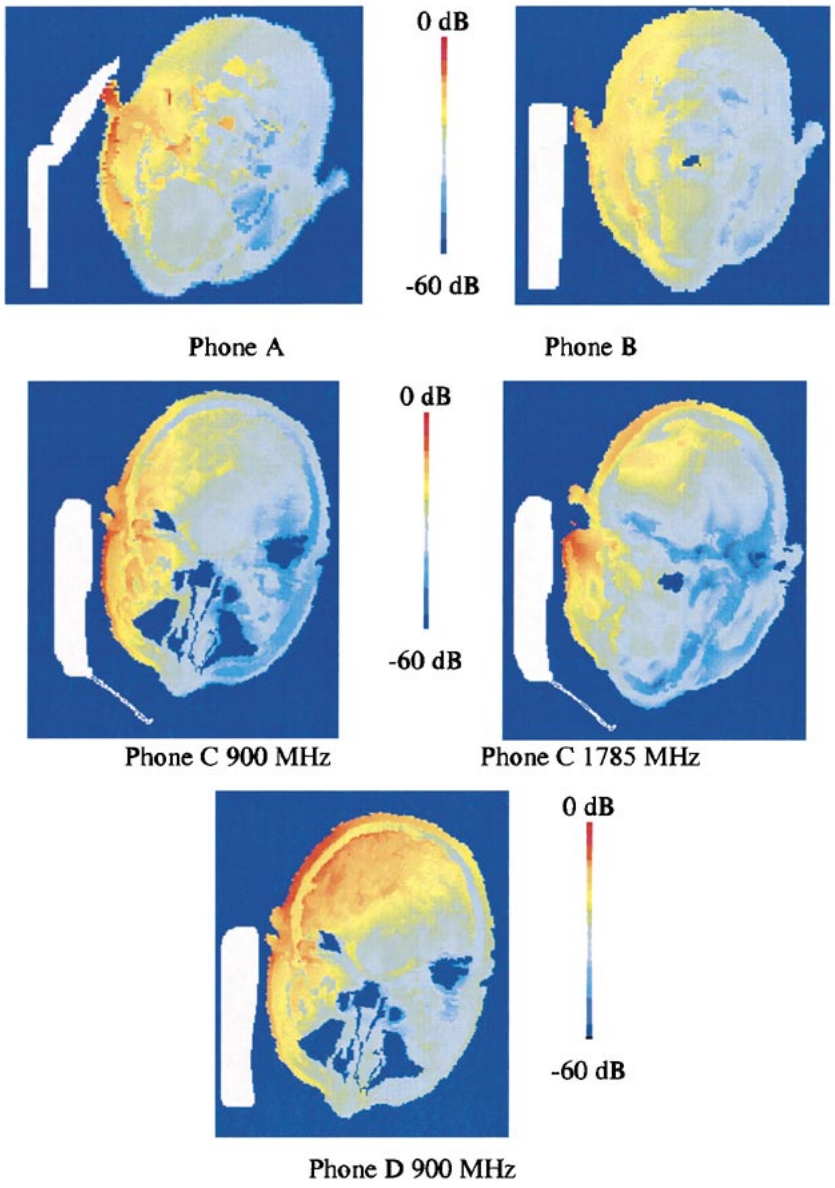

Fig. 8. SAR distribution inside a human head in logarithmic scale. The planes contain the maximum SAR.

TABLE V
COMPUTED SAR INSIDE A HUMAN HEAD

Phone	Frequency [MHz]	SAR_{peak} (1 cell) [W/kg]	$SAR_{1.0g}$ [W/kg]	$SAR_{10.0g}$ [W/kg]	P_{abs} [%]
Phone A	900	5.03	0.45	0.21	29.3
Phone B	900	4.82	0.30	0.21	29.4
Phone C	900	4.69	0.56	0.40	44.7
Phone C	1785	1.04	0.17	0.08	11.6
Phone D	900	1.00	0.15	0.11	20.2

TABLE VI
SAR PERCENTAGES (ABOVE 1%) IN EACH TISSUE

Tissue	Phone A [%]	Phone B [%]	Phone C 900 MHz [%]	Phone C 1785 MHz [%]	Phone D [%]
Skin	38.04	33.14	26.05	44.77	31.07
Muscle	19.54	15.83	29.44	12.94	15.33
Fat	5.67	4.70	9.01	5.63	3.29
Grey matter	10.28	15.35	9.79	10.18	16.47
Parotid Gland	4.05	1.92	5.20	6.86	1.40
White matter	6.93	9.18	5.90	5.23	10.46
CSF	8.86	11.78	6.87	6.39	12.49
Dry Bone	1.82	2.01	1.94	3.31	2.54
Pileum	1.32	2.49	1.66	2.61	3.82

The SAR generated by the same phones has been measured inside the homogeneous and inhomogeneous phantoms. To compare the measured SAR and the SAR computed inside the head, the power radiated by each phone has been measured (uncertainty on power measurement: ± 0.5 dB) and it has been used to scale the data shown in Table V. Since the measurement is performed in the brain equivalent liquid, the SAR has been computed only inside the brain region. Figs. 9 and 10 show a comparison on the averaged SAR; it also shows the uncertainty on the computed SAR due to the uncertainty in the power measurement. It can be observed that the measured SAR inside the homogeneous phantom is always higher than the SAR inside the inhomogeneous one. In general, the SAR measured inside the homogeneous phantom overestimate the SAR inside the human brain. Besides, measurements inside the inhomo-

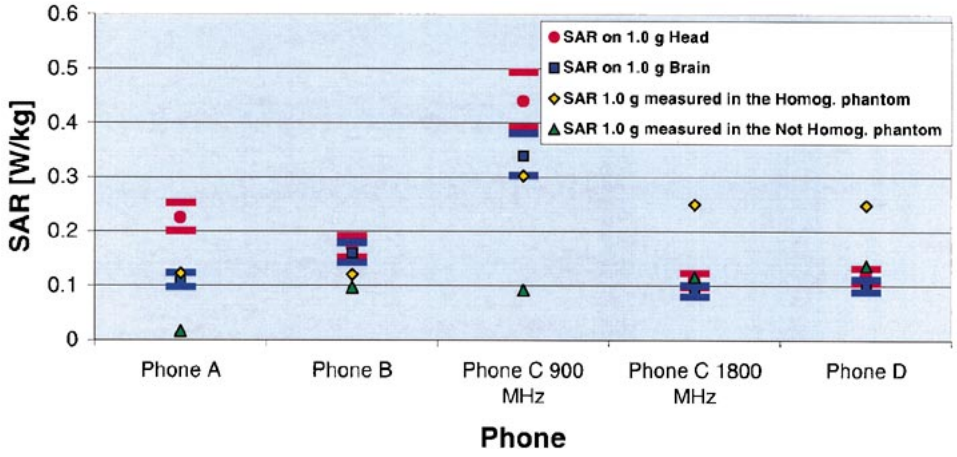

Fig. 9. Comparison between the SAR averaged on 1 g computed in a head and measured in phantoms.

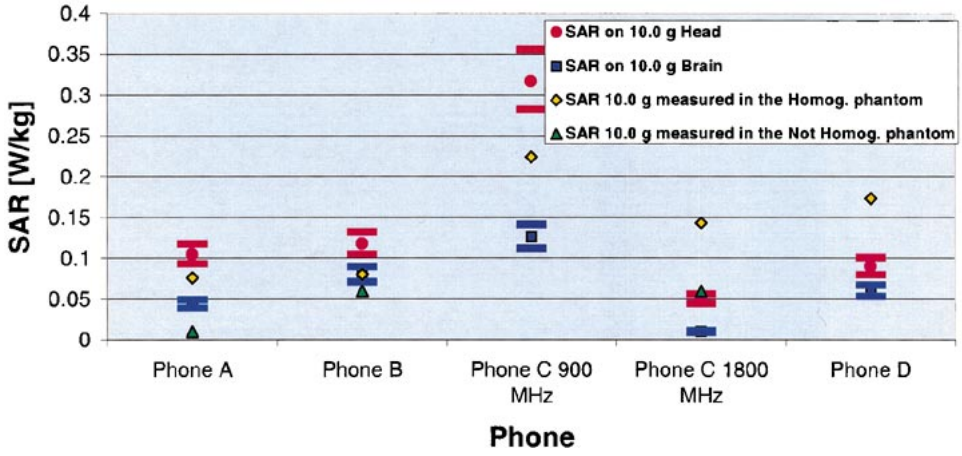

Fig. 10. Comparison between SAR averaged on 10 g computed in a head and measured in the phantoms.

geneous phantom are usually closer to the values computed in a human head. For phone C at 900 MHz and Phone D, the measured SAR on 10 g is not present since it is outside the area allowed for the probe's movement. The differences between the computed SAR into the head and measurements inside the phantoms are mainly due to the following:

- different phantoms/head dimensions;
- different physical constitution of the head and phantoms;
- different position/dimensions of the aperture on the phantoms;
- presence of the ear both on the head and the inhomogeneous phantom and its absence on the homogeneous phantom.
- different phone alignment with the phantoms and head due to the presence/absence of the ear and its dimensions.

VI. Conclusions

A procedure used to model cellular phones in their real shape, avoiding approximations, has been presented in this paper; it allows to manage the geometry of the phones without any manual action and to overcome the problem of the representation of general objects in a discretized space. The simplification in phone modeling as metallic boxes is no more necessary; on the other hand, correct modeling is important today when the shape of new cellular phones has a particular design imposed by market requirements. A comparison between measured and computed results has also been shown, both to validate the procedure in realistic phantoms and to demonstrate the reliability of the electromagnetic solver.

An anatomical model of a human head has been used to compute the SAR generated by four commercially available cellular phones at 900 and 1785 MHz. The SAR has been compared for the analyzed phones both in values and distribution, highlighting what tissues are more involved by radiation.

A comparison between the measured and computed SAR has been obtained for different phantoms and for a human head and the differences have been put in evidence. Remarkable differences have been found when using the same phone for measuring the SAR inside different phantoms.

The electromagnetic problem has been solved by using the FDTD technique; this approach can be used in the first stages of the design procedure of new phones to also take into account SAR constraints.

Acknowledgment

The authors wish to thank Dr. M. Crozzoli, Centro Studi e Laboratori di Telecommunicazioni, Turin, Italy.

REFERENCES

[1] *Consideration for Evaluation of Human Exposure to Electromagnetic Fields (EMF's) from Mobile Telecommunication Equipment (MTE) in the Frequency Range 30 MHz–6 GHz*, CENELEC Standard ES 59005, Oct. 1998.

[2] *IEEE Standard for Safety Levels with Respect to Human Exposure to Radio Frequency Electromagnetic Fields, 3 kHz to 300 GHz*, IEEE Standard C95.1-1991, 1991.

[3] M. A. Jensen and Y. Rahmat-Samii, "EM interaction of handset antennas and a human in personal communications," *Proc. IEEE*, vol. 83, pp. 7–17, Jan. 1995.

[4] O. P. Gandhi, J. Y. Chen, and D. Wu, "Electromagnetic absorption in the human head for mobile telephones at 835 and 1900 MHz," in *Proc. Int. EMC Symp.*, Rome, Italy, Sept. 1994, pp. 1–5.

[5] P. Bielli, A. Leoni, P. Massaglia, A. Schiavoni, S. Dionisi, F. Grimaldi, and P. Parente, "Expousre to hand-held transceiver radiation: Evaluation models and measurements," presented at the 6th Nordic Digital Mobile Radio Commun. Seminar, Stockholm, Sweden, June 1994.

[6] A. Watanabe, M. Taki, T. Nojima, and O. Fujiwara, "Characteristics of the SAR distributions in a head exposed to electromagnetic field radiated by a hand-held portable radio," *IEEE Trans. Microwave Theory Tech.*, vol. 44, pp. 1874–1883, Oct. 1996.

[7] A. Schiavoni, G. Richiardi, and P. Bielli, "SAR evaluation into an anatomically based model of the human head generated by different types of cellular phones," in *EMC'96*, Rome, Italy, Sept. 1996, pp. 182–187.

[8] A. Schiavoni and G. Richiardi, "FDTD analysis of the electromagnetic field into a human head like phantom and comparison with measurements," in *13th Int. Wroclaw Electromag. Compat. Symp. and Exhibition*, Wroclaw, Poland, 1996, pp. 25–28.

[9] M. Okoniewski and M. Stuchly, "A study of handset antenna and human body interaction," *IEEE Trans. Microwave Theory Tech.*, vol. 44, pp. 1855–1864, Oct. 1996.

[10] O. P. Gandhi, G. Lazzi, and C. M. Furse, "Electromagnetic absorption in the human head and neck for mobile telephones at 835 and 1900 MHz," *IEEE Trans. Microwave Theory Tech.*, vol. 44, pp. 1884–1897, Oct. 1996.

[11] C. M. Kuster, C. M. Balzano, and C. M. Lin, Eds., *Mobile Communication Safety*. ser. Telecommunications Technology and Applications. London, U.K.: Chapman & Hall, 1996.

[12] K. S. Kunz and R. J. Luebbers, *The Finite Difference Time Domain Method for Electromagnetic*. Boca Raton, FL: CRC Press, 1993.

[13] A. Taflove, *Computational Electrodynamics—The Finite Difference Time Domain Method*. Norwood, MA: Artech House, 1995.

[14] A. Tinniswood, C. M. Furse, and O. P. Gandhi, "Computations of SAR distribution for two anatomically based models of the human head using CAD files of commercial telephones and the parallelized FDTD code," *IEEE Trans. Antennas Propagat.*, vol. 46, pp. 829–833, June 1998.

[15] O. P. Gandhi, G. Lazzi, G. Tinniswood, and G. Yu, "Comparison of numerical and experimental methods for determination of SAR and radiation patterns of hand-held wireless telephones," *Bioelectromagnetics*, vol. 20, pp. 93–101, 1999.

[16] M. Annunziato, I. Bertini, and F. Matera, "Neural filter for segmentation of NMR images," in *9th SCIA*, June 1995.

[17] G. Richiardi, V. Vezzari, A. Schiavoni, P. Bertotto, and P. Bielli, "Numerical representation of cellular phones: Procedure and accuracy," in *EMC '98*, Rome, Italy, pp. 184–189.

[18] *Dielectric Data Base*. London, U.K.: MCL, 1995.

[19] G. Lazzi, C. M. Furse, and O. P. Gandhi, "FDTD computation of electromagnetic absorption in the human head for mobile telephones," in *BEMS'96*, Victoria, BC, Canada.

[20] S. Berntsen and S. N. Hornsleth, "Retarded time absorbing boundary conditions," *IEEE Trans. Antennas Propagat.*, vol. 42, pp. 1059–1064, Aug. 1994.

[21] K. Meier, O. Egger, T. Schmid, and N. Kuster, "Dosimetric laboratory for mobile communications," in *11th Int. EMC Tech. Exhibition Symp.*, Zurich, Switzerland, Mar. 1995, pp. 297–300.

[22] T. Schmid, O. Egger, and N. Kuster, "Automated E-field scanning system for dosimetric assessments," *IEEE Trans. Microwave Theory Tech.*, vol. 44, no. 1, pp. 105–113, Jan. 1996.

[23] N. Hartsgrove, N. Kraszewsky, and N. Surowiec, "Simulated biological materials for electromagnetic radiation absorption studies," *Bioelectromagnetics*, vol. 8, no. 1, pp. 29–36, 1987.

[24] *HP85070B Dielectric Probe Kit User's Manual*, Hewlett-Packard Company, Santa Rosa, CA, 1997.

[25] *Guide to Expression of Uncertainty in Measurement*, ISO TAG 4, 1993.

Andrea Schiavoni (S'87–M'87) was born in Jesi, Italy, in 1963. He received the electronic engineering and Ph.D. degrees from University of Ancona, Ancona, Italy, in 1990 and 1994, respectively.

From 1990 to 1993, he was with the University of Ancona, where he was involved with numerical modeling in electromagnetic compatibility. In 1993, he joined the Centro Studi e Laboratori Telecomunicazioni (CSELT), Turin, Italy, where he is currently involved theoretical and experimental dosimetry.

Paola Bertotto was born in Monfalcone, Italy, in 1969. She received the electronic engineering degree from the University of Trieste, Trieste, Italy.

In 1997, she joined the Centro Studi e Laboratori Telecomunicazioni (CSELT), Turin, Italy, where she is currently involved in experimental and theoretical dosimetry.

Gabriella Richiardi was born in Turin, Italy, in 1969. She received the information technology degree from the University of Torino, Turin, Italy, in 1995.

In 1996, she joined the Centro Studi e Laboratori Telecomunicazioni (CSELT), Turin, Italy, where she is currently involved in geometry modeling and developments of meshers for electromagnetic simulators.

Paolo Bielli, photograph and biography not available at time of publication.